

The subtle effect of integral scale on the drag of a circular cylinder in turbulent cross flow

Nibras Younis and David S.K. Ting*

Mechanical, Automotive & Materials Engineering University of Windsor Windsor, Ontario, Canada N9B 3P4
(Received April 7, 2011, Revised April 18, 2012, Accepted April 19, 2012)

Abstract. The effects of Reynolds number (Re), freestream turbulence intensity (Tu) and integral length scale (Λ) on the drag coefficient (C_d) of a circular cylinder in cross flow were experimentally studied for $6.45 \times 10^3 < Re < 1.82 \times 10^4$. With the help of orificed plates, Tu was fixed at approximately 0.5%, 5%, 7% and 9% and the normalized integral length scale (Λ/D) was varied from 0.35 to 1.05. Our turbulent results confirmed the general trend of decreasing C_d with increasing Tu . The effectiveness of Tu in reducing C_d is found to lessen with increasing Λ/D . Most interestingly, freestream turbulence of low Tu ($\approx 5\%$) and large Λ/D (≈ 1.05) can increase the C_d above the corresponding smooth flow value.

Keywords: circular cylinder; turbulence; cross flow; turbulence intensity; integral length scale; drag

1. Introduction

A cylindrical body in cross flow is a common scenario in nature and in widespread engineering applications. Circular cylinders are the basic component of transmission lines (Darwish *et al.* 2010), cables on cable-stayed bridges (Choi and Kim 2008, Raeesi *et al.* 2008), offshore structures (Pham *et al.* 2010), among many others. Even though the circular cylinder geometry is simple, the variety of flow phenomena and their interactions are very complex. It is no wonder that in spite of a century of intensive efforts, a circular cylinder in crossflow is still a popular research topic, especially via the numerical approach; see, for example, Zhao *et al.* (2011), Bhattacharyya and Singh (2011), Cao *et al.* (2010), Wang (2010), Singh and Mittal (2005).

When a single, smooth, rigid cylinder is subjected to a steady flow, distinct flow patterns occur within limited Reynolds number (Re) ranges called flow regimes. The start and end of these flow regimes can be specified by Reynolds number (Zdravkovich 1997). Fig. 1 illustrates the standard curve band for the drag coefficient versus Reynolds number. Four main flow regimes have been identified by Achenbach (1971) and confirmed by Zdravkovich (1997).

For $Re \leq 5$, streamlines firmly attach around the circumference with no visible wake behind the cylinder as portrayed in Fig. 2(a). The rear twin vortices begin to form at $Re \approx 5$ (Taneda 1956) and they become larger as Re increases; that is, the wake-length increases linearly with increasing Re (Coutanceau and Bouard 1977). The streamlines are steady and symmetrical with closed near-wake. At Reynolds number larger than approximately 30 the laminar wake starts to oscillate

* Corresponding author, Professor, E-mail: dting@uwindsor.ca

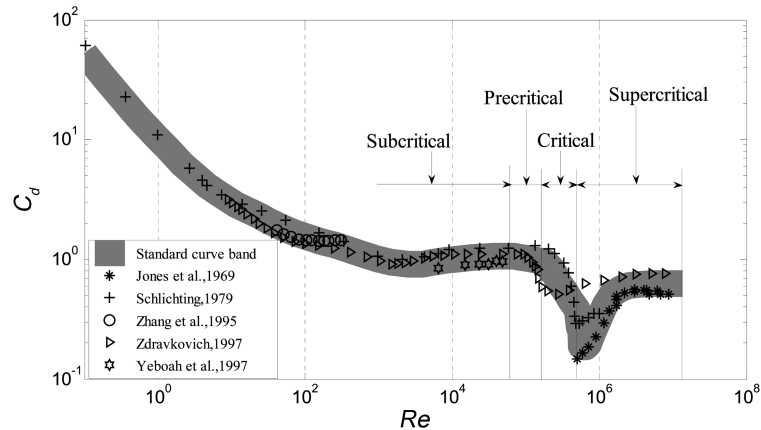


Fig. 1 Standard C_d - Re curve under 'smooth flow' condition

sinusoidally some distance downstream. This sinusoidal oscillation is initiated at the confluence point as a result of the instability of the elongated near-wake. The amplitude of the trail oscillation increases with Re , until a staggered array of laminar eddies are produced. This staggered array of laminar eddies is commonly referred to as the von-Karman vortex street; see Fig. 2(c). At a higher Reynolds number of about 180 the laminar periodic wake becomes unstable. Laminar and regular eddies become irregular and transitional farther downstream. The continuous distortion of laminar eddy ultimately leads to their breakdown. The subcritical regime covers a wide range of Re over which the drag coefficient remain literally unchanged at roughly 1.2; see Fig. 1.

With further increase in Re (to larger than 1×10^5 or so) the critical flow regime, where a sudden drop in the drag coefficient occurs, is approached. It is worth stressing that the occurrence of this regime varies somewhat from one study to another; see Fig. 1. Moreover, this general critical flow regime can be subdivided into sub-regimes. Zdravkovich (1997) described the $1 \sim 2 \times 10^5 < Re < 3 \sim 3.4 \times 10^5$ range where a single separation bubble is formed on one side of the cylinder, causing steady asymmetric pressure distribution, as the pre-critical regime. The formation of the second separation bubble and the return of flow symmetry takes place at $3 \sim 3.4 \times 10^5 < Re < 3.8 \sim 4 \times 10^5$. This is followed by the supercritical regime where the regular vortex shedding ceases ($5 \sim 10 \times 10^5 < Re < 3.6 \sim 6 \times 10^6$); see Fig. 2(e).

Real engineering applications are usually accompanied by different degrees of turbulence. The wake behind a circular cylinder is typically turbulent and so is the oncoming flow. Fage and Warsap (1929) found that the introduction of turbulence into the freestream causes the flow to behave as though it has a lower viscosity. In their wind tunnel under 'smooth flow' condition the resulting C_d - Re curve followed the standard curve; however, when a grid was introduced the drag reduced in varying degree depending on the grid characteristics and location. The general shape of the drag coefficient is not altered, but the curve is shifted toward a lower critical Re compared to the standard curve. In other words, turbulence promotes early transition to supercritical flow (Kiya *et al.* 1982, Blackburn and Melbourne 1996).

Researchers such as Ko and Graf (1972) and Arie *et al.* (1981) have mentioned the importance of turbulence scale in addition to turbulence intensity and Re in establishing the effects of turbulent freestream on the drag of a circular cylinder. Nevertheless, the general notion is that Tu is much more effective in lowering the critical C_d - Re range than integral length scale Λ (Mulcahy 1984). On

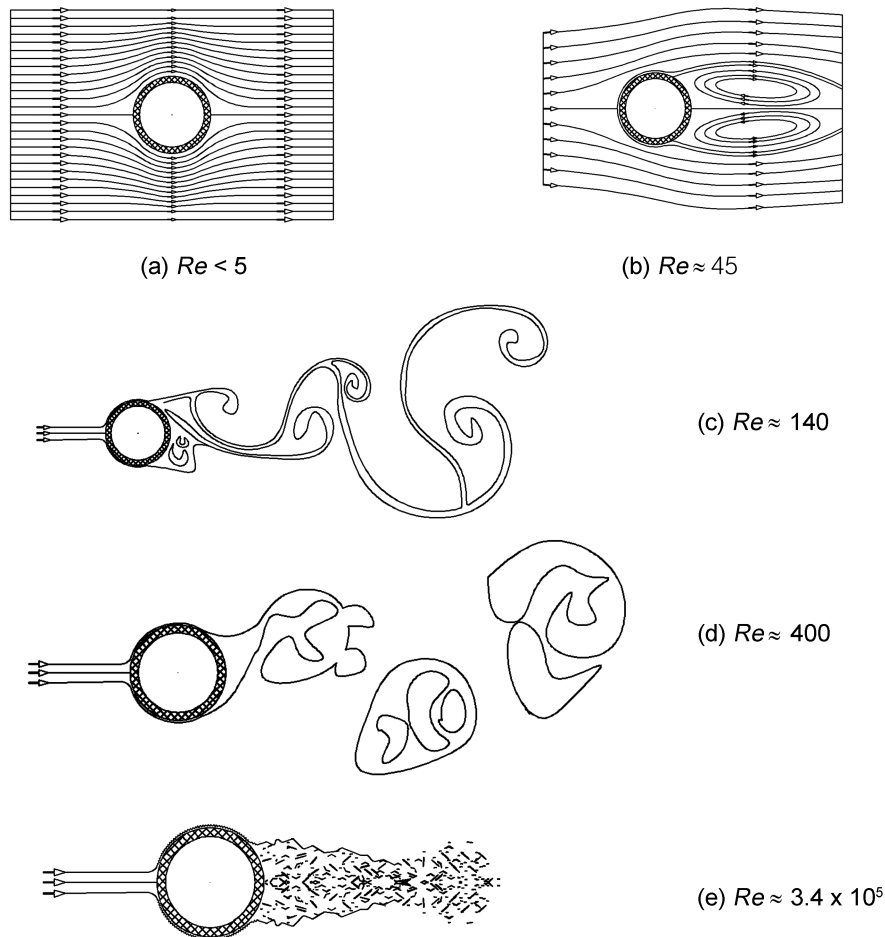


Fig. 2 Flow regimes of a circular cylinder in cross flow (a) $Re \leq 5$, (b) $Re \approx 45$, (c) $Re \approx 140$, (d) $Re \approx 400$ and (e) $Re \approx 3.4 \times 10^5$

the other hand, Ohya (2004) found that there is no difference in drag values on a circular cylinder in a highly turbulent atmosphere from those obtained in a 'smooth flow' wind tunnel. This seems to indicate that when $\Lambda/D \gg 1$ (where D is the diameter of the cylinder) the influence of turbulence diminishes. When the integral length is on the order of the diameter of the cylinder, on the other hand, there are significant quantitative and qualitative disagreements in the open literature. One reason behind these discrepancies is that care has not always been taken to keep other (turbulent) flow parameters consistent (fixed) when exploring the role of integral length scale. It is worth noting a relatively recent study by Zan (2008) in which two grids were used in generating 5% and 13% turbulence in a pressurized wind tunnel. The potential effect of the integral scale, however, was not discussed in this paper. Within the limits imposed by our experimental setup, we intend to independently disassociate the effect of turbulent integral length from those of Re and Tu in this study. This work is an extension from our previous work (Moradian *et al.* 2011), where a circular cylinder instead of a sphere is investigated in the current study.

2. Experimental details

The experiments were conducted in a closed-loop wind tunnel with a 4 m long test section. The cross section of this wind tunnel at the entrance is 0.762 m by 0.762 m. The cross-sectional area increases gradually downstream to overcome the boundary layer buildup on the wind tunnel walls. The maximum achievable mean velocity is approximately 20 m/s in the empty working section. The background flow turbulence is less than 0.5%.

The nominal freestream velocity was set via a Pitot-static tube connected to a digital manometer (Dwyer series 475 mark III), as illustrated in Fig. 3. The Pitot-static tube was removed and the small opening in the wind tunnel was sealed prior to taking hot-wire and force measurements.

The cylinder was positioned horizontally across the center line of the wind tunnel; see Fig. 3. At each end, an endplate was attached to the wall of the wind tunnel via a dummy section; a gap of 1~2 mm was maintained between the active cylinder and the endplate. A load cell was meticulously placed outside the left side (looking upstream) of the wind tunnel as depicted in Fig. 4. The load cell was an ATI six-axis force/torque sensor system (Gamma version SI-32-2.5) with a maximum load of 32 N. The load on the cylinder was conveyed via a shaft to the load cell. At the other end (right side when looking upstream), a ball and a socket were used to minimize the support system at this end from interfering with the load measurement taken at the left side. The endplate-dummy sections at both ends were secured to a rigid support outside the wind tunnel test section by two 12.5 mm thick aluminum angles.

The endplate dimensions were 7 D by 8 D, following the design suggested by Szepessy (1993). The leading edge was chamfered 20° according to Fox (1992); the distance between the leading edge and the center of the cylinder was 3.5 D and between the trailing edge and the cylinder center was 4.5 D. The endplates were placed 51 mm from the tunnel wall as per Stansby (1974), the center of the end plates together with the cylinder center coincided with the vertical midpoint of the wind tunnel. The endplates were made of acrylic and all the edges were smoothed by fine sand paper.

To check the load cell manufacturer calibration and the fact that the reading from only one load cell was accurate, a weight was placed at the center of the cylinder vertically. For the drag value the

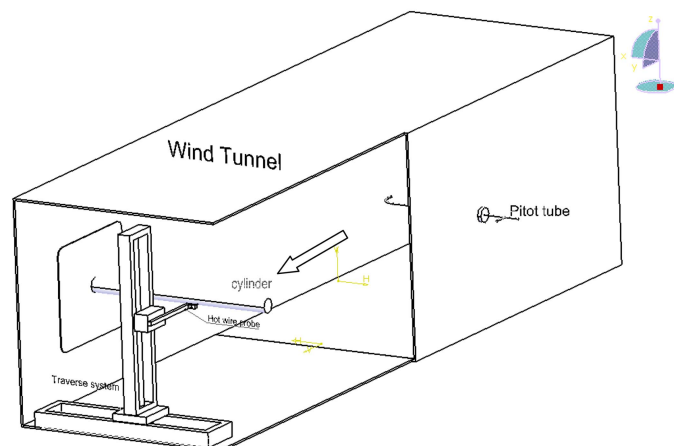


Fig. 3 Experimental setup

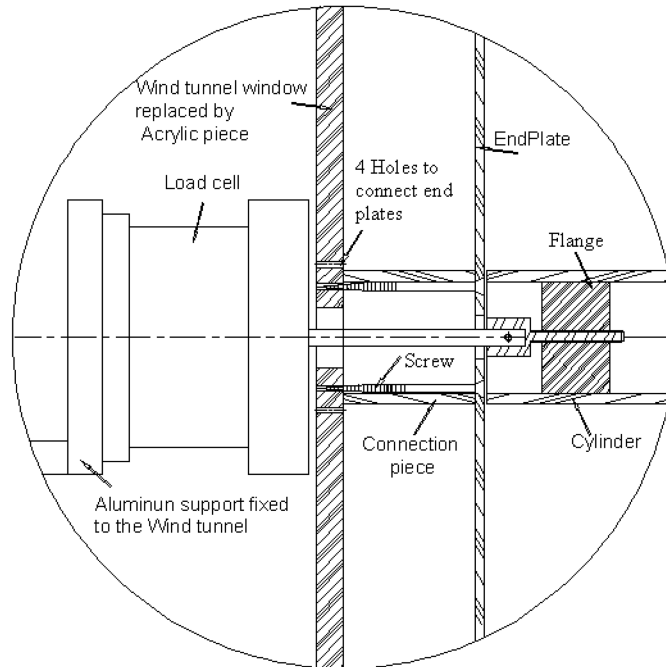


Fig. 4 The details of the end plate-load cell apparatus

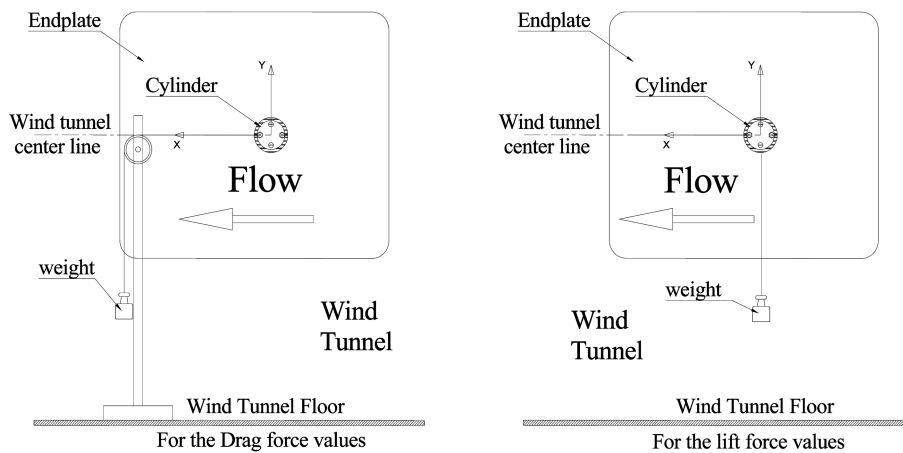
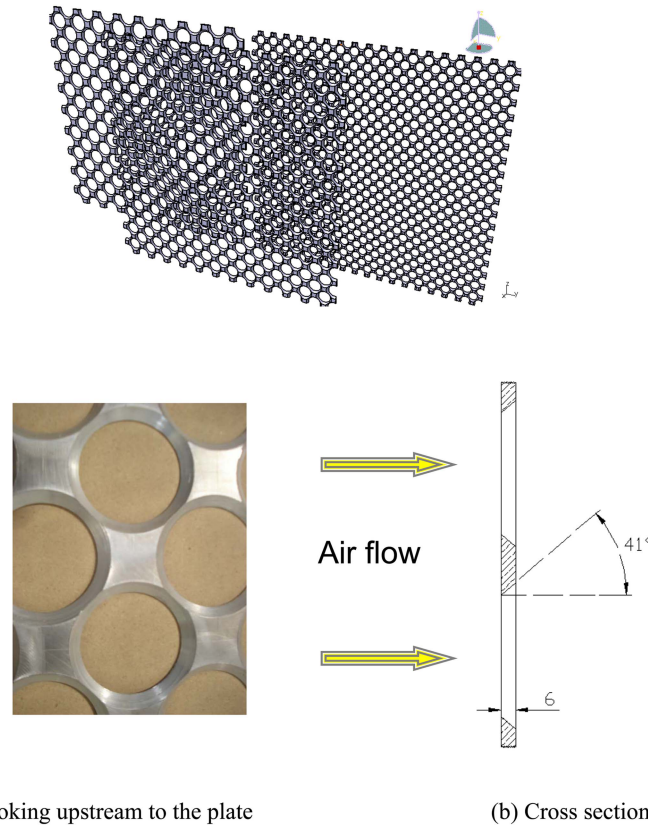


Fig. 5 Load cell calibration check

same procedure was repeated (in the x or drag direction), as shown in Fig. 5. Three weights (25 g, 50 g, and 100g) were used to check for the lift and drag calibrations supplied by the manufacturer, which were found to be sound.

Three cylinders with diameters of 26.7 mm, 33.6 mm, and 48.5 mm fabricated from ABS were employed. All three cylinders were sanded and polished to an average root mean square roughness value of $3.23 \mu\text{m}$. With respect to the smallest cylinder diameter (26.7 mm), the relative roughness was less than 0.0001; which is significantly smaller than the values considered by Achenbach (1971).



(a) Looking upstream to the plate

(b) Cross section of the plate

Fig. 6 The orificed perforated plates (a) Looking upstream to the plate and (b) Cross section of the plate

For flow velocity measurements, a one-dimensional hot-wire probe of DISA type 55p11 was connected to a Dantec Streamline 55C90 with a constant temperature hot-wire anemometer module installed within a Dantec 90N10 Frame. The one-dimensional hot-wire probe, together with the temperature probe, were mounted on a light-duty two-dimensional traversing system. The horizontal and vertical traverse lengths were 558 mm and 520 mm, respectively.

The fully computer-controlled calibration system consisted of a calibration Module (Dantec 90H10) placed in the Frame and a separate Flow Unit connected to the Calibration Module via a cable. The acceptable linearization errors were less than 1%. A sample size of 10^7 , beyond which the flow parameters of interest remained unchanged, was found to be adequate for the sampling frequency of 80 kHz. The signal was low-passed at 30 kHz to avoid aliasing problems.

The freestream turbulence was manipulated via the use of one of the three orificed perforated plates; see Fig. 6(a). These orificed perforated plates were machined from 6 mm thick aluminum plates. The three plates had holes of diameter $d = 25$ mm, 37.5 mm, and 50 mm, respectively. The solidity ratio of all three plates was maintained the same at 43%. All holes were machined into an orifice with a 41 angle; see Fig. 6. Liu *et al.* (2007) have shown that turbulent flow downstream of these orificed perforated plates is quasi-isotropic in nature.

3. Data analysis and procedure

The analog voltage output from the hot-wire system was digitized and converted to flow velocities according to the calibration curve. The time-averaged velocity is deduced as

$$\bar{U} = \sum_{i=1}^N \frac{U_i}{N} \quad (1)$$

where U_i is the instantaneous velocity (m/s) and N is the sample size.

The difference between the instantaneous velocity and the time-averaged velocity is the instantaneous fluctuating velocity. The root mean square value of this fluctuating velocity at any spatial location is calculated from

$$u_{rms} = \sqrt{\sum_{i=1}^N \frac{(U_i - \bar{U})^2}{N-1}} \quad (2)$$

The relative turbulence intensity is simply

$$Tu = \frac{u_{rms}}{\bar{U}} \times 100\% \quad (3)$$

The magnitude of integral length scale depends largely on the dimensions of the size of the holes and the spacing between them. It is evaluated from the area under the curve of the correlation function of the fluctuation velocity in the streamwise direction.

The integral time scale is computed using

$$\tau_A = \frac{\frac{1}{N-M} \sum_{i=1}^{N-M} (u_i u_{i+m})}{\frac{1}{N} \sum_{i=1}^N u_i^2} \quad (4)$$

Here M varies from 0 to $N-1$. The autocorrelation starts at one and the MatLab program stops when the autocorrelation first reaches a zero value. The area under the autocorrelation function is taken as the integral time scale. The integral length is estimated from this time by invoking Taylor frozen hypothesis, that is

$$A = \bar{U} \cdot \tau_A \quad (5)$$

3.1 Wind tunnel boundary layer

To minimize the wind tunnel boundary layer effect, endplates were meticulously designed according to specifications made by Stansby (1974), Fox (1992), and Szepessy (1993). Fig. 7 shows that over the range of velocity considered, the boundary layer was around 8 cm. Placing the endplates 51 mm from the walls led to a maximum velocity reduction from the freestream value of approximately 10% over a cylinder span of less than 8%.

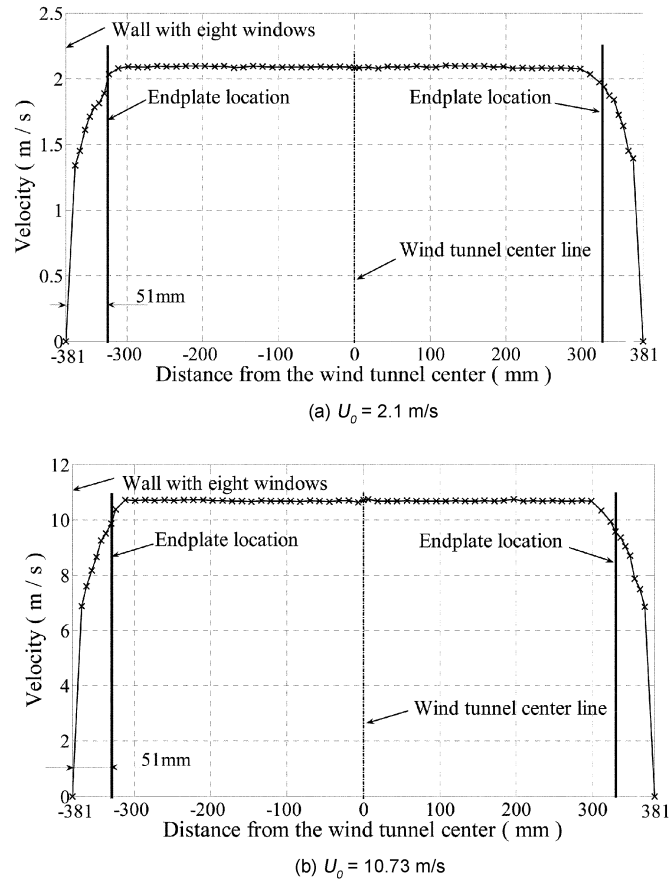


Fig. 7 Wind tunnel boundary layer check (a) $U_0 = 2.1$ m/s and (b) $U_0 = 10.7$ m/s

3.2 Endplate effects on C_d

The improvement in drag measurement with the utilization of the endplates is shown in Fig. 8. The control cylinder was the same active cylinder along with the two dummy ends, but without the two endplates. It is worth restating that the wind load on the dummy sections was not included in the measurement. Fig. 8 clearly depicts that C_d is reduced in the absence of endplates. Over the range of conditions considered, the drag coefficient increased somewhat when the endplates were used. By adding the endplates to the cylinder the wind tunnel boundary layer was significantly reduced and the flow passing the cylinder became more two dimensional. This result is consistent with those obtained by Stansby (1974) and Fox (1992) who confirmed the recovery of some drag in the presence of the endplates.

3.3 Blockage effects on C_d

As the cylinder spanned the wind tunnel test section, the blockage ratio is defined as the ratio of the diameter of the cylinder to the height of the test section. The maximum blockage ratio encountered in this experiment was 6%. According to West and Apelt (1982) noticeable flow

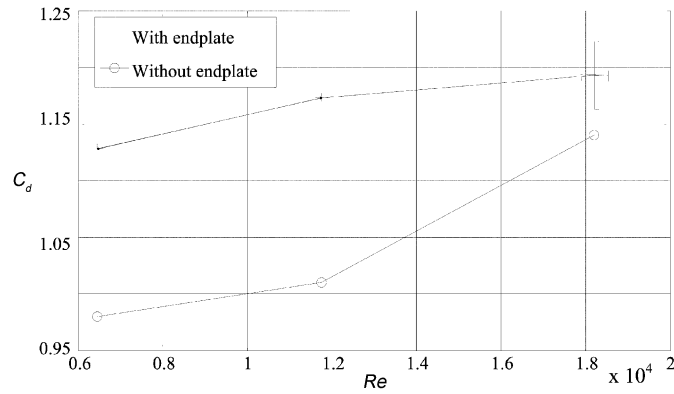


Fig. 8 Endplate effects on C_d

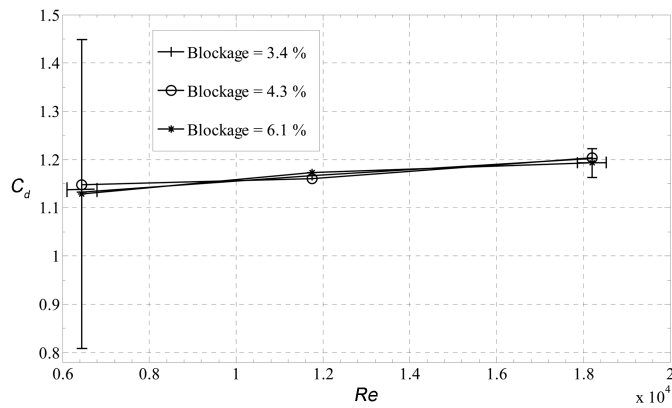


Fig. 9 Blockage effects on C_d

distortion occurs only when the blockage ratio is larger than 6%. To ensure that blockage was not an issue in the current experiment, the three cylinders with the corresponding endplates was tested for blockage effect. Fig. 9 shows that the value of the drag coefficient varied no more than the experimental uncertainty limits. Thus, no blockage correction was applied to the results obtained in this study.

3.4 The decay of turbulence downstream of the orificed perforated plate

The freestream turbulence intensity Tu and integral length scale Λ were manipulated with the help of the orificed perforated plates. To properly study the independent effects of Re , Tu and Λ/D , the parameter under investigation was varied over three different values while holding the other two parameters fixed. Thus, a test matrix of $3 \times 3 \times 3$ was generated. Eight different freestream velocities were chosen, and the characteristics of the orificed perforated plates for these eight velocities were found. For each velocity the turbulence intensity values along the center of the wind tunnel at 10, 15, 20, 30, and 40 diameters (of the holes of the orificed perforated plate) were deduced. Beyond a few diameters downstream of the plate, the flow turbulence decays in a power law manner. The obtained turbulence intensity results as plotted in Fig. 10 are consistent with Liu *et*

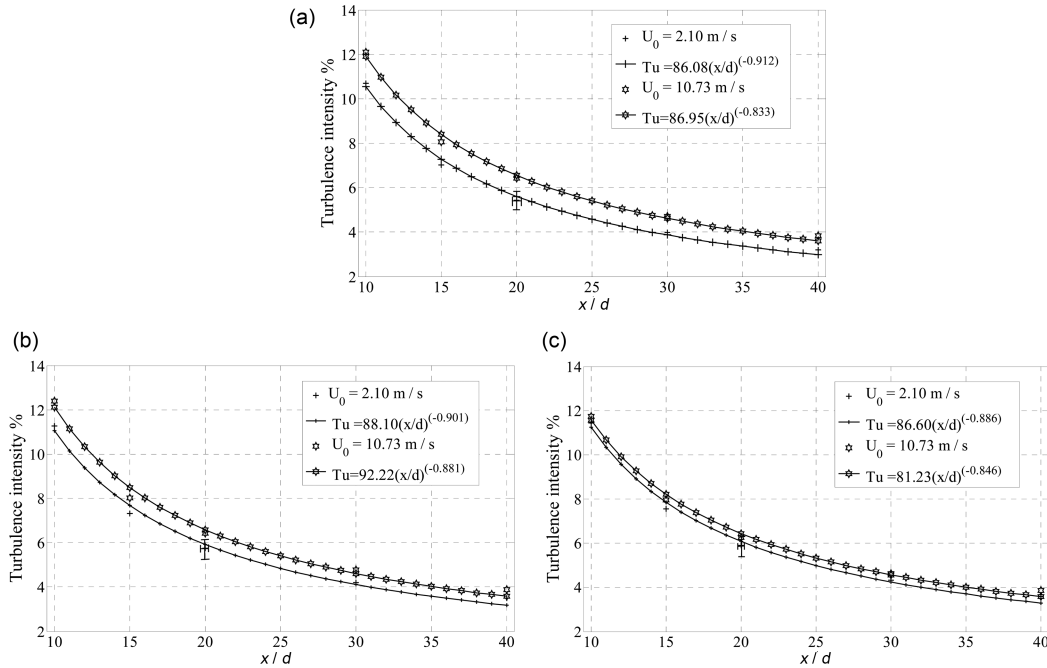


Fig. 10 Turbulence intensity downstream of (a) d25 plate, (b) d37.5 plate and (c) d50 plate

al. (2007). Note that the turbulence intensity is only marginally influenced by the wind speed, but it is a strong function of the location downstream of the orificed perforated plate. The Re uncertainty is estimated to be around ± 350 and ± 260 for Re of 6450 and 18200, respectively. Turbulence intensity uncertainty was around $\pm 0.5\%$ (absolute).

3.5 Integral length scale

Integral length scale signifies the average size of the energy containing eddies. The magnitude of integral length scale is mainly dependent on the size of perforation of the plate and the spacing between consecutive perforations. As for the turbulence intensity, sample integral length scale values associated with the five locations downstream of the orificed perforated plates are plotted in Fig. 11. Over the range of conditions considered, the variation in integral length scale downstream of the perforated plate is approximately linear, for this reason a linear curve fit is employed to fit each data set associated with a particular wind speed. Fig. 11 depicts that the integral length scale depends slightly on Re , moderately on d , and strongly on the distance downstream of the orificed perforated plate. The relative integral length scale uncertainty was estimated to be 12%.

3.6 Re matrix

To achieve three repeating Re values, eight velocities along with three different cylinder sizes were needed. To fix Tu at 5%, 7%, and 9%, the corresponding distances between the orificed perforated plates and the center of the cylinder were selected based on both the power law curve fit for Tu and the linear curve fit for Λ . In other words, to attain a particular Tu the corresponding plate

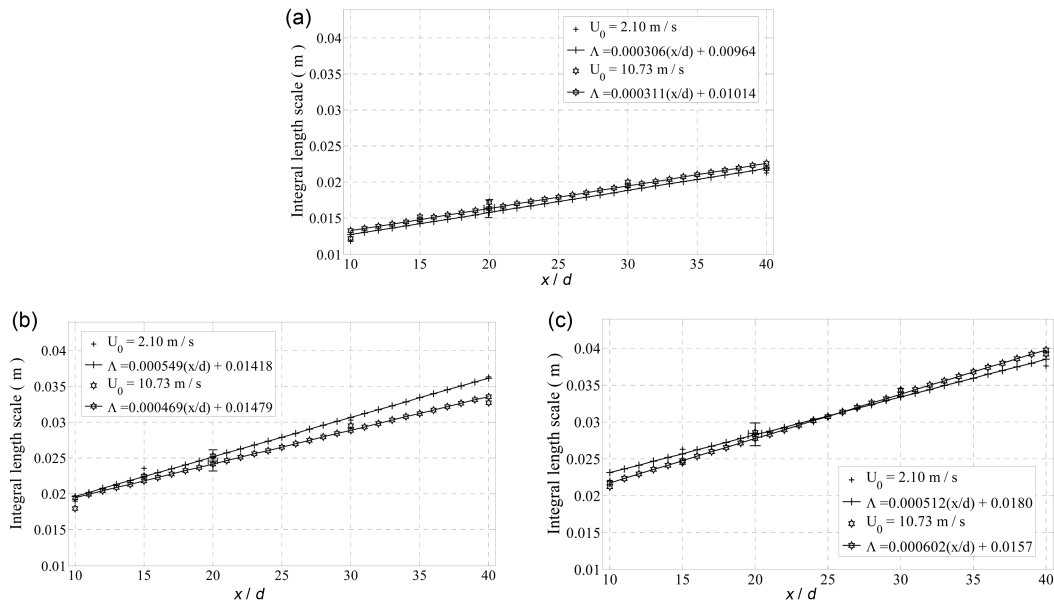


Fig. 11 Integral length scale downstream of (a) d25 plate, (b) d37.5 plate and (c) d50 plate

location (upstream of the cylinder) was obtained from the Tu curve fit equation. Subsequently, the required value of Λ for this perforated plate and the plate-cylinder distance was determined from the linear Λ fit.

4. Results and discussion

Efforts were made in choosing the particular conditions (wind velocity, perforated plate, plate-cylinder distance, and cylinder diameter) for supplying at least three data points to portray the independent roles of Re , Tu and Λ/D . To compare the turbulence results with those in the 'no turbulence' ('smooth flow') scenario, drag measurements were also taken in the absence of the orificed perforated plate.

The turbulence intensity in the wind tunnel in the absence of the orificed perforated plate was measured to be less than 0.5%, therefore the measured drag is expected to behave as the standard C_d-Re curve obtained by the earlier researchers. The C_d-Re results obtained are plotted in Fig. 12. The current results fall within the 'smooth flow' C_d versus Re standard curve limits. The uncertainties in the drag coefficient measurement were estimated to be around ± 0.3 and ± 0.03 for Re of 6450 and 18200, respectively.

4.1 The effect of freestream turbulence

In the literature, the main consensus concerning the role of freestream turbulence is the advancement of the drag crisis with increasing turbulence intensity; see, for example, Fage and Warsap (1929), Bruun and Davies (1975), Savkar *et al.* (1980), Blackburn and Melbourne (1996), and Sanitjai and Goldstein (2001). The other general agreement is the typical reduction in the drag coefficient with

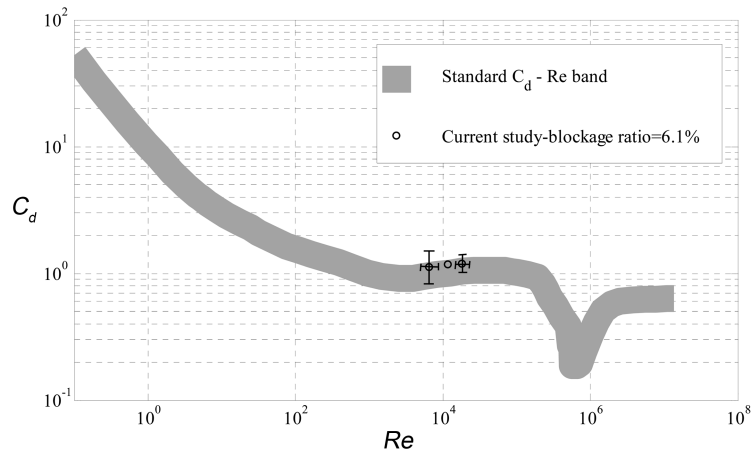


Fig. 12 Present 'smooth flow' results with respect to the standard curve

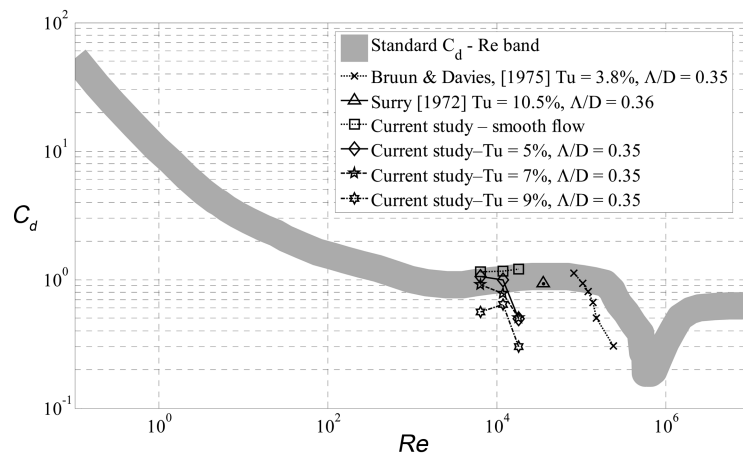


Fig. 13 The general effect of turbulence on C_d - Re curve

increasing turbulence intensity (Bearman 1968, Arie *et al.* 1981). Our results as plotted in Fig. 13 are consistent with these earlier studies in the sense that for fixed Λ/D , the drag typically decreases and the sudden drop associated with the drag crisis occurs at smaller Re , with increasing turbulence intensity (from $< 0.5\%$ to 5% to 7%).

4.2 The effect of Reynolds number

The drag coefficient for fixed Tu and Λ/D is plotted as a function of Re in Fig. 14. Note that as the absolute uncertainties of the underlying parameters remain roughly unchanged with wind speed and/or cylinder size, the resulting relative uncertainty of C_d becomes significantly larger with decreasing Re , especially at the lowest tested Re . Fig. 14(a) shows that for $\Lambda/D = 1.05$ there appears to be a marginal increase in C_d with Re , over the range of conditions considered. More interestingly, the C_d associated with Tu of 5% is noticeably larger than the corresponding C_d under 'smooth flow' condition, particularly at $Re = 1.2 \times 10^4$ and at the largest tested Re (where the $Tu = 7\%$ point is also

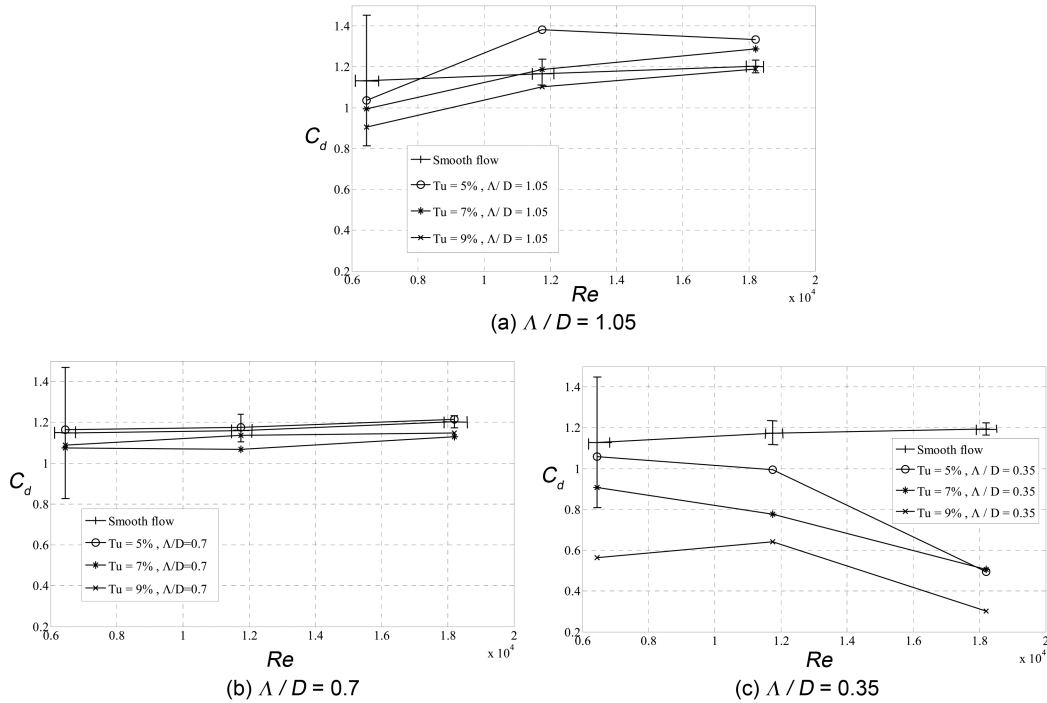


Fig. 14 The effects of Re on C_d (a) $\Lambda/D = 1.05$, (b) $\Lambda/D = 0.7$ and (c) $\Lambda/D = 0.35$

larger). A couple of earlier researchers have also detected this phenomenon. Savkar *et al.* (1980) have found that for Λ/D of 1.3, Tu of 9.5% and $Re \sim 10^4$, the value of C_d can be larger than the corresponding standard value under ‘smooth flow’ condition, and that C_d can drop below the standard value at higher Re . Arie *et al.* (1981) have noted when $\Lambda/D > 1$ the drag coefficient tends to be larger than the standard values, and this trend is reversed as Λ/D is reduced. Our results as plotted in Fig. 14(b) show that, for the range of conditions considered in this study, this ‘crossover point’ of Re effect on C_d occurs at $\Lambda/D \approx 0.7$. Consistent with Arie *et al.* (1981), our $\Lambda/D \approx 0.35$ results in Fig. 14(c) clearly depict decreasing C_d with increasing Re . In short, the drag coefficient increases with Re when Λ/D is larger than one and it decreases with Re when Λ/D is less than unity.

4.3 The subtle effect of integral length scale

Surry (1972) suggested that the turbulence scale has a couple of effects: a) a direct effect on the change of the position of the boundary layer separation points and b) an influence on the flow outside the boundary layer, including the wake. The turbulent C_d data obtained in this study are plotted against Λ/D in Fig. 15. The most obvious general trend is the increase in C_d with Λ/D for the three levels of turbulence considered; or more correctly, C_d decreases as Λ/D is reduced below unity.

Keeping in mind that the standard C_d values over the range Re investigated here are around 1.2, we see that some C_d data points for Λ/D of approximately unity are somewhat above the ‘smooth flow’ values, as shown in Fig. 14. This is particularly the situation for the larger Re cases with $Tu = 5\%$, Fig. 15(a). Fig. 15(a) seems to show for Re of 6450 the general trend of increasing C_d with Λ/D is only true when increasing Λ/D from 0.35 to 0.7; further increase in Λ/D from 0.7 to 1.05 actually

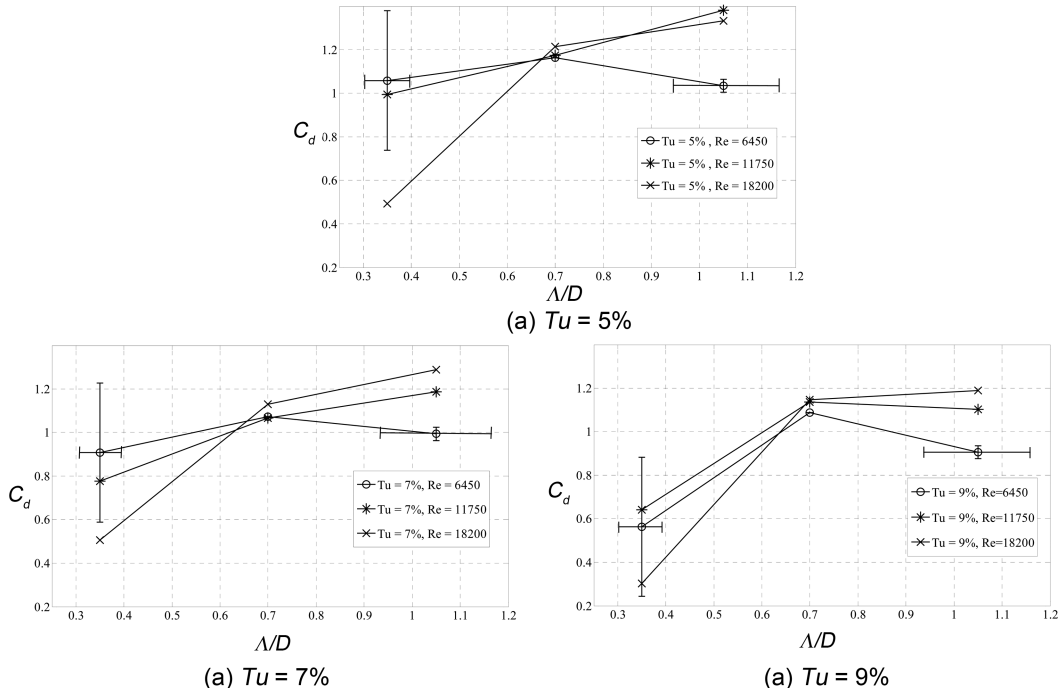


Fig. 15 The effects of Λ/D on C_d (a) $Tu = 5\%$, (b) $Tu = 7\%$ and (c) $Tu = 9\%$

results in a reduction in C_d . This increase-decrease C_d with increasing Λ/D behavior is also detected when $Re = 6450$ and $Tu = 7\%$ (Fig. 15(b)), and for both $Re = 6450$ and $Re = 1.2 \times 10^4$ with $Tu = 9\%$ (Fig. 15(c)). In other words, Λ/D of unity (0.7) appears to be a transition point where the qualitative effect of integral length scale on C_d reverses under some situations. The significant reduction in C_d when lowering Λ/D below the ‘critical’ value of 0.7 is particularly obvious.

4.4 The effects of Re , Tu and Λ/D

To depict the three-fold effects of Re , Tu and Λ/D , C_d is plotted against Re and Λ/D , with constant Tu data points connected as contour surfaces in Fig. 16. The general trend of decreasing drag with increasing turbulence intensity is clearly seen from the constant Tu contours. The decreasing C_d with increasing Re characteristic is also easily detectable, noting again that with moderately low turbulence ($Tu = 5\%$) C_d increases above the corresponding standard values before it decreases with increasing Re . Also readily seen in Fig. 16 is the general decreasing C_d with decreasing Λ/D trend, particularly at large Re (and Tu). It is worth stressing the apparent critical Λ/D of 0.7, below which C_d decreases with decreasing Λ/D , but above which C_d may increase with decreasing Λ/D , especially at small Re .

Current findings are put into perspective with those obtained by a couple of eminent researchers in Fig. 17. Among many others, Bruun and Davies (1975) have confirmed that for the same value of Λ/D and Tu , the drag coefficient decreases with increasing Re . The advancement of the drag crisis is the most agreeable result among the many researchers in this field.

As referred to before, Arie *et al.* (1981) have discovered that when $\Lambda/D \approx 2$ and turbulence intensity relatively high at 12.3% (the inverted triangles in Fig. 17), the drag coefficient value is

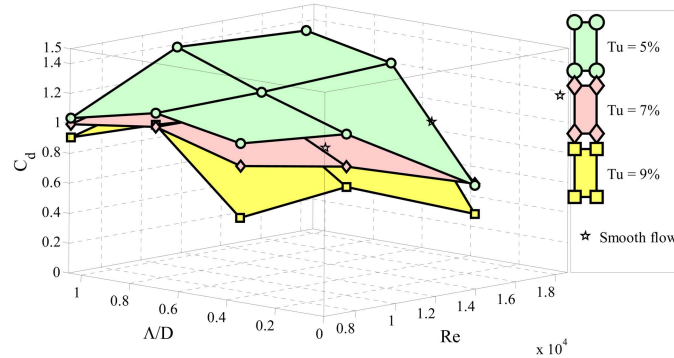


Fig. 16 The effects of Re , Tu and Λ/D on C_d

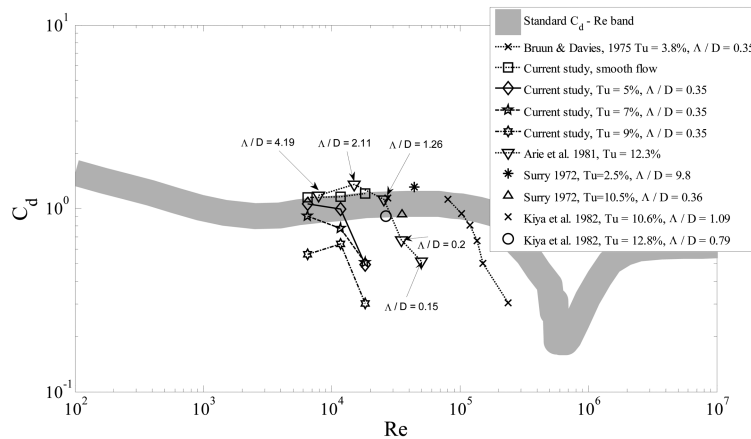


Fig. 17 A comparison of drag results

roughly the same as their corresponding ‘smooth flow’ value. Similarly, Surry’s (1972) data revealed that when $\Lambda/D \approx 9.8$ with relatively low turbulence intensity of 2.5%, the drag coefficient value is higher than that obtained in ‘smooth flow’; however, when Λ/D is decreased to 0.36 the corresponding drag coefficient drops below the smooth flow value. Furthermore, Kiya *et al.* (1982) have observed that the drag of the cylinder in turbulent freestream with $\Lambda/D = 1.09$ and $Tu = 10.6\%$ is larger than that when $\Lambda/D = 0.79$ and $Tu = 12.8\%$. These studies confirm that increasing Tu can lead to an increase in drag when Λ/D is large (>1), and that certain higher-than-unity Λ/D conditions can compromise (and even reverse) the drag reduction effect caused by freestream turbulence. At smaller Λ/D values (<1), however, the general trend of decreasing drag coefficient with increasing turbulence intensity prevails.

5. Conclusions

The independent effects of freestream Reynolds number, turbulence intensity, and the integral length scale/cylinder diameter ratio on the drag of a circular cylinder in cross flow were

experimentally investigated. The investigation was conducted in a closed-loop wind tunnel over a Reynolds number range of 6.45×10^3 to 1.82×10^4 . The proper combination of orificed perforated plate holes diameter, cylinder location with respect to the orificed perforated plate and the wind speed in the wind tunnel enabled the quasi-independent alterations of Reynolds number, turbulence intensity, and relative integral length scale. The current results have confirmed the most obvious observation of advancing drag crisis with increasing turbulence intensity. Also affirmed is the general trend of decreasing drag with increasing turbulence intensity. It is interesting to note that the drag can increase above the corresponding 'smooth flow' values under some turbulent conditions. Most interestingly, it is found that λ/D can seriously enhance the effectiveness of turbulence in decreasing the drag when it is reduced, particularly below a critical value of approximately 0.7.

Acknowledgements

This work was made possible by NSERC (Natural Sciences and Engineering Research Council of Canada).

References

- Achenbach, E. (1971), "Influence of roughness on the cross-flow around a circular cylinder", *J. Fluid Mech.*, **46**(2), 321-335.
- Arie, M., Kiya, M., Suzuki, Y., Hagino M. and Takahashi, K. (1981), "Characteristics of circular cylinders in turbulent flows", *Bull. Japan Soc. Mech. Eng.*, **24**(190), 640-647.
- Bhattacharyya, S. and Singh, A.K. (2011), "Reduction in drag and vortex shedding frequency through porous sheath around a circular cylinder", *Int. J. Numer. Meth. Fl.*, **65**(6), 683-698.
- Bearman, P.W. (1968), *Some effects of turbulence on the flow around bluff bodies*, National Physical Laboratory, Aerodynamics division, Report 1264.
- Blackburn, H.M. and Melbourne, W.H. (1996), "The effect of free-stream turbulence on sectional lift forces on a circular cylinder", *J. Fluid Mech.*, **306**, 267-292.
- Bruun, H.H. and Davies, P.O. (1975), "An experimental investigation of the unsteady pressure forces on a circular cylinder in a turbulent cross flow", *J. Sound Vib.*, **40**(4), 535-559.
- Cao, S., Ozono, S., Tamura, Y., Ge Y. and Kikugawa, H. (2010), "Numerical simulation of Reynolds number effects on velocity shear flow around a circular cylinder", *J. Fluid Struct.*, **26**(5), 685-702.
- Choi, S.W. and Kim, H.K. (2008), "Design of aerodynamics stabilizing cables for a cable-stayed bridge during construction", *Wind Struct.*, **11**(5), 391-411.
- Coutanceau, M. and Bouard, R. (1977), "Experimental determination of the main features of the viscous flow in the wake of a circular cylinder in uniform translation. I. Steady flow", *J. Fluid Mech.*, **79**(2), 231-256.
- Darwish, M.M., El Damatty, A. and Hangan, H. (2010), "Dynamic characteristics of transmission line conductors and behaviour under turbulent downburst loading", *Wind Struct.*, **13**(4), 327-346.
- Fage, A. and Warsap, J.H. (1929), *The effects of turbulence and surface roughness on the drag of a circular cylinder*, Aeronautical Research Committee, Reports and Memoranda No. 1283.
- Fox, T.A. (1992), "End plate interference effects on the aerodynamics of a circular cylinder in uniform flow", *Aeronaut. J.*, **96**(951), 10-14.
- Jones, G., Cinotta, J. and Walker, R. (1969), *Aerodynamic forces on a stationary and oscillating circular at high Reynolds number*, NACA TR R-300.
- Kiya, M., Suzuki, Y., Arie, M. and Hagino, M. (1982), "A contribution to the free-stream turbulence effect on the flow past a circular cylinder", *J. Fluid Mech.*, **115**, 151-164.
- Ko, S.C. and Graf, W.H. (1972), "Drag coefficient of cylinders in turbulent flow", *J. Hydraul. Eng. - ASCE*,

- 98(5), 897-912.
- Liu, R., Ting, D.S.K. and Checkel, M.D. (2007), "Constant Reynolds number turbulence downstream of an orificed perforated plate", *Exp. Therm. Fluid Sci.*, **31**(8), 897-908.
- Moradian, N., Ting, D.S.K. and Cheng, S. (2011), "Advancing drag crisis of a sphere via the manipulation of integral length scale", *Wind Struct.*, **14**(1), 35-53.
- Mulcahy, T.M. (1984), "Fluid forces on a rigid cylinder in turbulent cross flow", *Proceedings of the American Society of Mechanical Engineers*, Winter Ann. Meeting, New Orleans 15-28.
- Ohya, Y. (2004), "Drag of circular cylinders in the atmospheric turbulence", *Fluid Dyn. Res.*, **34**, 135-144.
- Pham, A.H., Lee, C.Y., Seo, J.H., Chun, H.H., Kim, H.J., Yoon, H.S., Kim, J.H., Park, D.W. and Park, II-R. (2010), "Laminar flow past an oscillating circular cylinder in cross flow", *J. Marine Sci. Technol.*, **18**(3), 361-368.
- Raeesi, A., Cheng, S. and Ting, D.S.K. (2008), "Spatial flow structure around a smooth circular cylinder in the critical Reynolds number regime under cross-flow condition", *Wind Struct.*, **11**(3), 221-240.
- Sanitjai, S. and Goldstein, R.J. (2001), "Effect of free stream turbulence on local mass transfer from a circular cylinder", *Int. J. Heat Fluid Fl.*, **44**, 2863-2875.
- Savkar, S.D., So, R.M. and Litzinger, T.A. (1980), *Fluctuating lift and drag forces induced on large span bluff bodies in a turbulent cross flow*, American Society of Mechanical Engineers, Heat Transfer Division, (Publication) HTD, 9, 19-26.
- Schlichting, H. (1979), *Boundary Layer Theory*, McGraw-Hill
- Singh, S.P. and Mittal, S. (2005), "Flow past a cylinder: shear layer instability and drag crisis", *Int. J. Numer. Meth. Fl.*, **47**(1), 75-98.
- Stansby, P.K. (1974), "The effects of end plates on the base pressure coefficient of a circular cylinder", *Aeronaut. J.*, **78**, 36-37.
- Szepessy, S. (1993), "On the control of circular cylinder flow by end plates", *Euro. J. Mech. B Fl.*, **12**(2), 217-244.
- Surry, D. (1972), "Some effects of intense turbulence on the aerodynamics of a circular cylinder at subcritical Reynolds number", *J. Fluid Mech.*, **52**(3), 543-563.
- Taneda, S. (1956), "Experimental investigation of the wake behind cylinders and plates at low Reynolds numbers", *J. Phys. Soc. Jpn.*, **11**(3), 302-307.
- Wang, J.S. (2010), "Flow around a circular cylinder using a finite-volume TVD scheme based on a vector transformation approach", *J. Hydrodynamics*, **22**(2), 221-228.
- West, G.S. and Apelt, C.J. (1982), "The effects of the tunnel blockage and aspect ratio on the mean flow past a circular cylinder with Reynolds number between 10^4 and 10^5 ", *J. Fluid Mech.*, **114**, 361-377.
- Yeboah, E.N., Rahai, H.R. and LaRue, J.C. (1997), *The effects of external turbulence on mean pressure distribution, drag coefficient, and wake characteristics of smooth cylinders*, ASME Fluids Engineering Division Summer Meeting, FEDSM'97-3167
- Zan, S.J. (2008), "Experiments on circular cylinders in crossflow at Reynolds numbers up to 7 million", *J. Wind Eng. Ind. Aerod.*, **96**(6-7), 880-886.
- Zdravkovich, M. (1997), *Flow around Circular Cylinders*, Oxford University Press.
- Zhao, M., Cheng, L. and Zhou, T. (2011), "Three-dimensional numerical simulation of oscillatory flow around a circular cylinder at right and oblique attacks", *Ocean Eng.*, **38**(17-18), 2056-2069.
- Zhang, H.Q., Fey, U., Noack, B.R., Konig, M. and Eckelmann, H. (1995), "On the transition of the cylinder wake", *Physics Fluid*, **7**(4), 779-794.

CC

Nomenclature

A	Cylinder frontal area, $A = \text{length} \times \text{diameter}$ (m^2)
C_d	Nondimensional drag coefficient, $C_d = \frac{2F_d}{\rho U_0^2 A}$

d	Orificed, perforated plate holes diameter (mm)
D	Cylinder diameter (mm)
F_d	Drag force (N)
N	Sample size
Re	Reynolds number, $Re = \frac{\rho U_0 D}{\mu}$
rms	Root mean square
Tu	Turbulence intensity $\frac{u_{rms}}{\bar{U}}$
U	Instantaneous velocity (m/s)
U_0	Free stream velocity (m/s)
\bar{U}	Time-averaged velocity (m/s)
u_{rms}	Root mean square velocity (m/s)

Greek Symbols

Λ	Integral length scale (mm)
μ	Dynamic viscosity $\left(\frac{\text{kg}}{\text{m} \cdot \text{s}}\right)$
ρ	Fluid density (kg/m^3)
τ_Λ	Integral time scale (s)